Journal of Magnetic Resonance 196 (2009) 191–199

Contents lists available at ScienceDirect

Journal of Magnetic Resonance

journal homepage: www.elsevier.com/locate/jmr

Application of shaped adiabatic pulses to MQMAS NMR spectroscopy of spin 3/2 nuclei

David Rovnyak *, Paul E. Kennedy

Bucknell University, Department of Chemistry, Moore Avenue, Lewisburg, PA 17837, USA

ARTICLE INFO

Article history:
Received 3 July 2008
Revised 2 November 2008
Available online 18 November 2008

Keywords:
MQMAS
Multiple-quantum magic-angle spinning
RIACT
Adiabatic coherence transfer
Sodium
Quadrupole

ABSTRACT

Competition between nutation (r.f. driven) and adiabatic (rotor-driven) multi-quantum coherence transfer mechanisms in spin 3/2 systems results in diminished performance of rotation induced adiabatic coherence transfer (RIACT) in isotropic multiple-quantum magic-angle spinning (MQMAS) experiments for small e^2qQ/h (<2 MHz) and high radio-frequency powers. We present a simple shaped RIACT pulse consisting of a truncated sine wave (spanning 0–0.8π) that corrects the sensitivity losses, phase twist and relative intensity errors that can arise in MQMAS spectra utilizing constant-amplitude RIACT pulses. The shaped RIACT pulse may enhance the study of metals in biomolecules where quadrupole couplings of $S = 3/2$ nuclei such as ^{23}Na tend to be small.

1. Introduction

A great deal of activity has been devoted to improving the efficiency of multi- quantum (MQ) coherence transfers of half-integer quadrupolar nuclei in order to improve the sensivity and information content of the isotropic multiple-quantum magic-angle spinning (MQMAS) experiment [1–4]. The MQMAS experiment has been of broad value in the study of condensed phases, giving researchers the option to exploit diverse nuclei as exquisitely sensitive reporters on local structure [3,4]. Briefly, the principal experimental concerns in MQMAS are the excitation of a symmetric multi-quantum coherence (e.g. connecting $\pm m_S$ states, where $m_S = 3/2, 5/2, ...$) of half-integer quadrupolar nuclei and the subsequent conversion of the MQ coherence to central transition (CT) coherence. A great deal of progress has been made in developing methods to improve the efficiency of these two basic steps of MQMAS (review articles [3,4]). A closely related experimental approach is the satellite transition magic-angle-spinning (STMAS) experiment [5,6] which also provides isotropic spectra for half-integer quadrupolar nuclei. While offering a number of desirable performance characteristics such as enhanced sensitivity and quantitative accuracy, STMAS yields less intrinsic resolution in the isotropic dimension than MQMAS for $S = 3/2$ nuclei and is sensitive to small mis-settings of the magic-angle. In this work, we are interested in observing ^{23}Na, which is 100% abundant, exhibits small quadrupole couplings, and has a gyromagnetic ratio similar to carbon-13. Further, poor chemical shift dispersion is observed among sodium cations so that the enhanced resolution in the isotropic dimension of MQMAS due to the contribution of the second order quadrupole coupling can be valuable in discerning distinct sites such as DNA bound sodium cations [7–10]. It appears at this time that the MQMAS approach is advantageous for detecting abundant nuclei with high gyromagnetic ratios such as ^{23}Na in biomolecules, while STMAS is advantageous for nuclei with small magnetogyric ratios and low natural abundances [11,12].

The use of rotation induced adiabatic coherence transfer [13] (RIACT) in MQMAS significantly enhanced the sensitivity of nuclei with e^2qQ/h greater than about 2.0 MHz and provided isotropic lines whose relative intensities corresponded to site populations of crystallographically distinct species, with integer precision (i.e. correct values are obtained when relative signal intensities are rounded to nearest integer values) [14]. The initial report of adiabatic coherence transfers to enhance the MQMAS experiment focused on the value of achieving coherence transfer that is largely insensitive to the magnitude of the quadrupole coupling [14]. For sodium sites exhibiting large quadrupole couplings (e.g. e^2qQ/h >2.0 MHz), the sensitivity of their MQMAS spectra were enhanced often several fold by the RIACT mechanism compared to MQMAS spectra obtained with short high power pulses (a.k.a. nutation) to drive multi-quantum coherence transfers. The performance of RIACT in the case of quadrupole couplings (e.g. e^2qQ/h <2.0 MHz) was not considered in detail, which is the focus of this work.

In this study we demonstrate for spin 3/2 nuclei that the RIACT mechanism is undermined by competing nutation mechanisms as e^2qQ/h decreases and as the r.f. power increases. Adverse effects

* Corresponding author. Fax: +1 570 577 1739.
E-mail address: drovnyak@bucknell.edu (D. Rovnyak).

1090-7807/$ - see front matter © 2008 Elsevier Inc. All rights reserved.
doi:10.1016/j.jmr.2008.11.005

resulting from this competition among the nutation and RIACT transfer mechanisms are phase twist, diminished sensitivity, and loss of quantitative accuracy in RIACT MQMAS spectra. We show it is possible to significantly suppress unwanted nutation pathways by the use of simple amplitude modulated pulses, and thereby select for pure adiabatic coherence pathways. By exerting this control over coherence transfer pathways, the shaped RIACT pulse restores quantitative accuracy, moderately enhances sensitivity, and eliminates phase twist in MQMAS spectra of sites with e^2qQ/h <2 MHz for ^{23}Na ($S = 3/2$).

2. Theory

We examine mechanisms for generating triple quantum coherence for a half-integer quadrupolar nucleus.

2.1. Nutation in the triple quantum subspace

We review first the nutation of Zeeman polarization of a spin 3/2 quadrupolar nucleus. In this case, an r.f. pulse is applied to an initial condition of the equilibrium polarization of central and triple quantum transitions; this case has been well characterized [15–17] and was widely exploited during the initial development of MQMAS methodology [1,18,19]. We review the approach of Vega in using fictitious spin-1/2 operators to describe the nutation of triple quantum coherence for an $S = 3/2$ nucleus in the regime of $\omega_Q > \omega_1$, where ω_Q (defined below) is proportional to the magnitude of the quadrupole coupling and $\omega_1 = \gamma B_1$ represents the strength of the applied r.f. field [15]. We treat the other limiting case $\omega_1 > \omega_Q$ in the Appendix, but discuss the result in this section. Sample rotation is not considered, which may be viewed as the static case, or as a short-time treatment since nutation is observed over just a few microseconds (e.g. compared to a 100 μs rotor period at 10 kHz MAS).

The rotating frame Hamiltonian for a $S = 3/2$ nucleus under r.f. irradiation and in the fictitious spin-1/2 basis is [13,15,16]

$$H^Q_{LAB} = -\Delta\omega(3\mathbf{I}^{14}_Z + \mathbf{I}^{23}_Z) + \omega_Q(\mathbf{I}^{12}_Z - \mathbf{I}^{34}_Z) - \omega_1(\sqrt{3}\mathbf{I}^{12}_X + 2\mathbf{I}^{23}_X + \sqrt{3}\mathbf{I}^{34}_X), \quad (1)$$

where ω_1 is the magnitude of the r.f. field, ω_Q is the quadrupole coupling frequency,

$$\omega_Q = \frac{e^2qQ/h}{6}\left(\frac{1}{2}(3\cos^2\theta - 1) + \eta\sin^2\theta\cos 2\phi\right), \quad (2)$$

and θ and ϕ are Euler angles relating the principal axes system (PAS) of the quadrupolar tensor to the laboratory (LAB) frame. Spin angular momentum operators are given in boldface for fictitious spin-1/2 transitions where the 2–3 superscript denotes the central transition and the 1–2 and 3–4 superscripts denote the satellite transitions. The offset term $\Delta\omega$ will be neglected. In this first case, we will monitor 3Q coherence if the initial condition is equilibrium polarization (ignoring constants for convenience):

$$\rho_{LAB}(0) \propto \mathbf{I}_Z = \mathbf{I}^{23}_Z + 3\mathbf{I}^{14}_Z. \quad (3)$$

In Eq. (1) the 1–2 subspace is tilted away from $\mathbf{I}^{12}_Z$ by $\theta_{12} = \tan^{-1}[\frac{\sqrt{3}\omega_1}{\omega_Q}]$ and the 3–4 subspace is tilted by $\theta_{34} = -\tan^{-1}[\frac{\sqrt{3}\omega_1}{\omega_Q}]$ away from $-\mathbf{I}^{34}_Z$. Setting $\theta = \theta_{12} = -\theta_{34}$, the doubly tilted frame Hamiltonian is

$$H^Q_{TILT} = \omega_{eff}\left(\mathbf{I}^{12}_Z - \mathbf{I}^{34}_Z\right) - \omega_1\left[2\cos^2\left(\frac{\theta}{2}\right)\mathbf{I}^{23}_X + 2\sin^2\left(\frac{\theta}{2}\right)\mathbf{I}^{14}_X + \sin(\theta)\mathbf{I}^{13}_X + \sin(\theta)\mathbf{I}^{24}_X\right], \quad (4)$$

where $\omega_{eff} = (\omega_Q^2 + 3\omega_1^2)^{1/2}$. Next assume that

$$\rho_{TILT}(0) \cong \rho_{LAB}(0) = \mathbf{I}^{23}_Z + 3\mathbf{I}^{14}_Z. \quad (5)$$

The limiting condition $\omega_Q > \omega_1$ gives[15]

$$H^Q_{TILT}(\omega_Q >> \omega_1) \cong \omega_{eff}\left(\mathbf{I}^{12}_Z - \mathbf{I}^{34}_Z\right) - \omega_1 2\mathbf{I}^{23}_X + \frac{3\omega_1^3}{2\omega_Q^2}\mathbf{I}^{14}_X + \frac{\sqrt{3}\omega_1^2}{\omega_Q}\left(\mathbf{I}^{13}_X + \mathbf{I}^{24}_X\right). \quad (6)$$

Commutation relations [15,16] show that the $(\mathbf{I}^{13}_X + \mathbf{I}^{24}_X)$ term will not produce 3Q coherence from an initial density operator of $(\mathbf{I}^{23}_Z + 3\mathbf{I}^{14}_Z)$. The term in Eq. (6) governing triple quantum coherence excitation is $H^Q_{TILT}(\omega_Q >> \omega_1) \cong \frac{3\omega_1^3}{2\omega_Q^2}\mathbf{I}^{14}_X$, which will nutate the triple quantum term of Eq. (5) only; it is a sensitive function of ω_1, and is attenuated quadratically by ω_Q. The dependence of nutation on ω_1 and ω_Q is well supported by computational and empirical optimizations of coherence transfers for MQMAS [1,18,19].

A very similar approach is employed in the Appendix to obtain the following expression incorporating the opposite limiting condition $\omega_1 > \omega_Q$,

$$H^Q_T = -2\omega_1\mathbf{I}^{23}_X - \frac{\omega_Q^2}{6\omega_1}\mathbf{I}^{14}_X + \omega_{eff}\left(\mathbf{I}^{12}_X + \mathbf{I}^{34}_X\right) - \frac{\omega_Q}{\sqrt{3}}\left(\mathbf{I}^{13}_X + \mathbf{I}^{24}_X\right). \quad (7)$$

In Eq. (7) it can be seen that nutation in the triple quantum subspace now depends *directly* on the square of the quadrupole frequency, and this behavior was qualitatively investigated previously [7]. Achieving this limit in practice is challenging since even quadrupole couplings that would be considered small in the sense that they yield MAS line shapes that are too narrow to show typical shoulders and horns characteristic of the quadrupolar interaction tensor (e.g. $e^2qQ/h \sim 0.5$ MHz) nonetheless have quadrupole frequencies on the order of 10^3 kHz.

2.2. Nutation of the central transition

We consider applying an r.f. pulse to central transition coherence and monitoring the creation of triple quantum coherence. This situation arises in a two pulse experiment in which the first pulse employs low power to selectively excite central transition coherence, while the second is a 90-degree phase-shifted high power pulse. Although this scheme will lead to adiabatic rotor-driven coherence transfer during the second pulse, [13,14,20] we are interested in the question: if the initial density operator is $\rho(0) \propto \mathbf{I}^{23}_X$, can there be r.f. driven triple quantum excitation?

In the limiting condition $\omega_Q > \omega_1$, the term $\frac{\sqrt{3}\omega_1^2}{\omega_Q}(\mathbf{I}^{13}_X + \mathbf{I}^{24}_X)$ in Eq. (6) leads to triple quantum coherence when acting upon $\mathbf{I}^{23}_X$, which can be seen using $e^{iA}Be^{-iA} = B + i[A,B] - \frac{1}{2}[A,[A,B]] + \ldots$ and taking $A = \mathbf{I}^{13}_X + \mathbf{I}^{24}_X$ and $B = \mathbf{I}^{23}_X$ (e.g. see Ref. [21]). However with $\omega_Q > \omega_1$, the factor $\frac{\sqrt{3}\omega_1^2}{\omega_Q}$ can become much smaller than w_1. We expect then that nutation of the central transition into 3Q coherence will be a minor mechanism when $\omega_Q > \omega_1$, and will show that simulations verify this as well.

In the limiting condition $\omega_1 > \omega_Q$, the term $\omega_{eff}(\mathbf{I}^{12}_X + \mathbf{I}^{34}_X) - \frac{\omega_Q}{\sqrt{3}}(\mathbf{I}^{13}_X + \mathbf{I}^{24}_X)$ leads to triple quantum coherence. To obtain a rough approximation, the last part can be neglected, giving the nutation of 3Q coherence proportional to $\omega_{eff} = (\omega_Q^2 + 3\omega_1^2)^{1/2}$ which approaches $\sqrt{3}\omega_1$. In either limiting condition, we note again that these predictions are useful only for predicting initial nutation rates since we consider static conditions.

In this work we are especially interested in $S = 3/2$ nuclei in the regime $e^2qQ/h = 0.5 - 2.0$ MHz subjected to r.f. powers on the order of 100–150 kHz, so that ω_Q and ω_1 are of the same order of magnitude and neither of the above conditions is fully satisfactory.

An alternative that may be less sensitive to extreme limiting conditions in ω_1 and ω_Q is to consider the r.f. Hamiltonian in a quadrupolar interaction frame [15,21]. Ignoring resonance offsets in Eq. (1), if we take the quadrupole interaction to define the unitary transformation

$$U = e^{i\omega_Q t(\mathbf{I}_Z^{12} - \mathbf{I}_Z^{34})}, \tag{8}$$

and evaluate

$$\tilde{H}_{rf} = U^{-1}\hat{H}_{rot}U, \tag{9}$$

then one obtains [15,21]

$$\tilde{H}_{rf} = 2\omega_1\mathbf{I}_X^{23} + \sqrt{3}\omega_1\cos(\omega_Q t)\left(\mathbf{I}_X^{12} + \mathbf{I}_X^{34}\right) + \sqrt{3}\omega_1\sin(\omega_Q t)\left(\mathbf{I}_Y^{12} - \mathbf{I}_Y^{34}\right). \tag{10}$$

Particularly for very small r.f pulse powers, the contribution of the time dependent terms of Eq. (10) may be neglected, allowing for $\tilde{H}_{rf} \cong 2\omega_1\mathbf{I}_X^{23}$ to selectively spin-lock the central transition [13]. Importantly, the time dependent terms must be considered as ω_1 increases. The terms $(\mathbf{I}_X^{12} + \mathbf{I}_X^{34})$ and $(\mathbf{I}_Y^{12} - \mathbf{I}_Y^{34})$ generate triple quantum coherence from an initial condition of central transition coherence; MAS modulation of these terms leads to rotor-driven coherence transfer [15,21,22]. And simulations show that r.f. driven 3Q excitation results from the use of the Hamiltonian of Eq. (10) (*vide infra*) and must originate from these terms as well. For example, we see that Eqs. (7) and (10) converge as ω_1/ω_Q increases, and in taking the instantaneous behavior ($t \sim 0$) in Eq. (10). Analytically extending Eq. (10) to longer times does not appear to be straightforward, [21] and future work to better understand the competing coherence transfer processes is warranted. Nonetheless, Eq. (10) suggests that the instantaneous (i.e. $t \sim 0$) r.f. driven excitation of 3Q coherence from an initial condition of $\mathbf{I}_X^{23}$ will be on the order of $\sqrt{3}\omega_1$.

2.3. Rotation induced adiabatic coherence transfer is insensitive to ω_Q for $\omega_Q > \omega_1$

Under combined sample rotation and r.f. irradiation, the central transition coherence of a half-integer nucleus will be adiabatically modulated by the time dependence of the first order quadrupole coupling [13]. The first order quadrupole coupling under sample rotation is [13]

$$Q(t) = \frac{\omega_Q(t)}{2} = \frac{\omega_Q}{2}\left[-\sqrt{2}\sin(2\beta)\cos(\omega_r t + \gamma) + \sin^2\beta\cos(2\omega_r t + 2\gamma)\right], \tag{11}$$

where β relates the principal axis of the electric field gradient tensor to the axis of sample rotation, γ is a rotation (phase) about the spinning axis, and ω_r is the frequency of rotation. The time dependence of $Q(t)$ drives an oscillation of the eigenstates of the Hamiltonian between the outermost symmetric coherence and the central transition coherence with either one or two periods per rotor cycle.

Two conditions must be fulfilled to observe adiabatic coherence transfer. First we have $\omega_Q > \omega_1$ so that the central transition coherence and outer symmetric coherence (e.g. triple quantum in $S = 3/2$ or quintuple for $S = 5/2$) are good eigenstates of the Hamiltonian [13]. Second, the modulation of the Hamiltonian must be sufficiently slow such that the nuclear spin states adiabatically follow the changing eigenstates of the time dependent Hamiltonian. An adiabaticity test parameter [13]

$$\alpha = \frac{\omega_1^2}{\omega_Q\omega_r} >> 1 \tag{12}$$

describes when this second condition is fulfilled. In practice, meeting this condition amounts to using r.f. field strengths that significantly exceed the MAS rate. For example, high r.f. powers are necessary for driving adiabatic coherence transfers in nuclei with large quadrupole couplings [14]. Provided high r.f. powers can be attained, Eq. (12) indicates that rotation induced adiabatic coherence transfers (RIACT) are insensitive to the magnitude of the quadrupole coupling. Notably, Eq. (12) predicts that the condition for adiabatic transfer will improve for decreasing ω_Q (provided $\omega_Q > \omega_1$ still holds).

Increasing ω_r decreases α and therefore threatens meeting the adiabatic condition in Eq. (12). The practical reality is that r.f. power levels in small diameter solenoidal coils (e.g. employing sample rotors of 2.5 or 3.2 mm diameters) and for high gamma nuclei such as ^{11}B or ^{23}Na can easily reach 130–150 kHz (expressing power as a nutation rate). Even for MAS rates up to 25 kHz, as in this study, maintaining $\alpha > 1$ is straightforward and there is little dependence of RIACT efficiencies on MAS rates, which we will show.

In summary, when the initial condition is equilibrium polarization, r.f nutation in the triple quantum subspace will be the dominant contribution to the excitation of 3Q coherence. When the initial condition is central transition coherence, a superposition of r.f. nutation and adiabatic processes generate 3Q coherence.

3. Experimental

All samples were obtained from commercial sources and were used without further purification. All salts were white powders, but were ground using a mortar and pestle to insure uniformly polycrystalline morphology. All experiments were performed on a Varian Inc. (Palo Alto, CA) DirectDrive spectrometer operating at 14.1 T (158 MHz for ^{23}Na) and employing a 3.2 mm diameter rotor. Spectra were not locked nor corrected for lock as drift is about 0.1 Hz/h for ^{23}Na. All spectra were processed using the Rowland NMR Toolkit (rnmrtk) [23].

The pulse sequences used in this study are illustrated in Fig. 1. A basic triple quantum filtering experiment is shown in Fig. 1a,

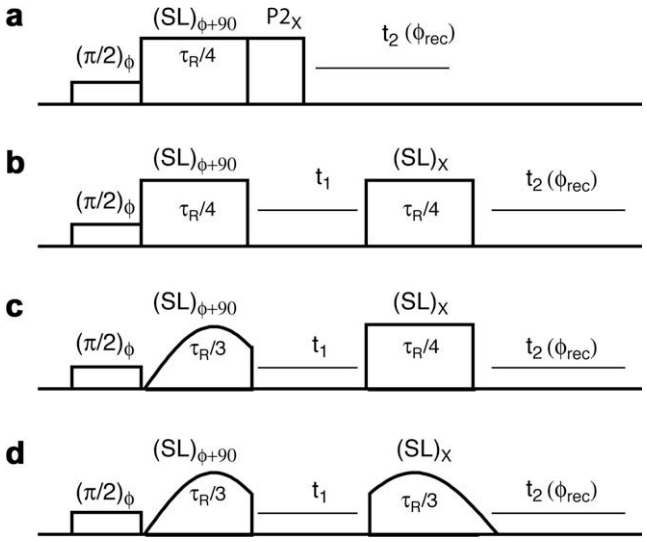

Fig. 1. Pulse sequences used in this study are (a) a triple quantum filter for monitoring excitation of triple quantum coherence generated by the action of a spin-locking pulse (SL), and (b–d) rotation induced adiabatic coherence transfer MQMAS experiments, often termed RIACT(II)-MQMAS to indicate that the RIACT mechanism is employed for both excitation and reconversion of multi-quantum coherence. In all experiments, ϕ is incremented in 30° steps and the receiver in 90° steps to select for the triple quantum coherence transfer pathway. The shaped pulse is a truncated sine wave (0–0.8π) with an optimal duration of $\tau_R/3$.

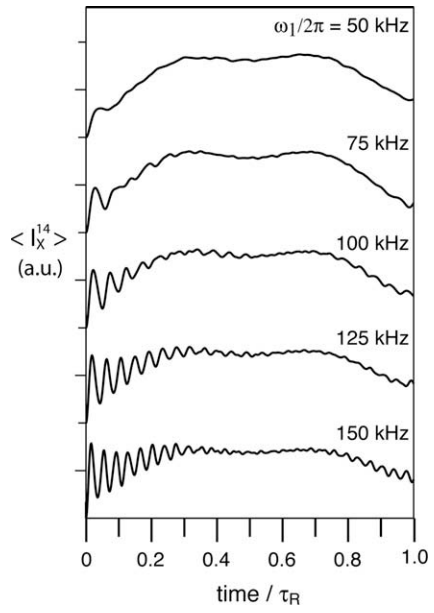

Fig. 2. Numerical simulations of triple quantum coherence excitation over one rotor period (100 μs) given an initial condition of $\rho(0) = \mathbf{I}_x^{23}$ and employing only the low order quadrupolar coupling in the Hamiltonian (i.e. $\propto A_{20}T_{20}$ in spherical tensor notation). High frequency oscillations dependent on the applied r.f. power (ω_1) demonstrate nutation processes superimposed upon RIACT. The simulations also assumed 10 kHz MAS, e^2qQ/h = 1.0 MHz, η = 0.0, and 2000 crystal orientations.

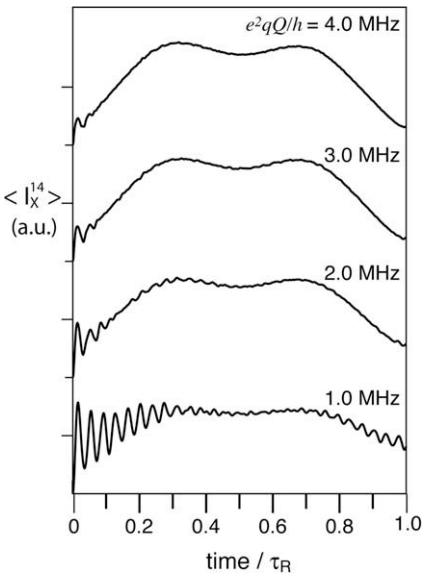

Fig. 3. Numerical simulations of triple quantum coherence excitation using identical conditions as in Fig. 2, except for varying the value of e^2qQ/h and fixing $\omega_1/2\pi$ = 150 kHz. Decreasing the quadrupole coupling favors the nutation process.

where the initial creation of 3Q coherence is accomplished by a RIACT module consisting of a selective $\pi/2$ pulse on the central transition and a 90-degree phase-shifted pulse of duration $\tau_r/4$, which gives optimal coherence transfer; [14,24] a nutation pulse in Fig. 1a reconverts the 3Q coherence to central transition coherence. Several straightforward variations on Fig. 1a will also be employed. A MQMAS experiment incorporates an indirect evolution period following triple quantum excitation,[1,2] as shown in Fig. 1b where both excitation and reconversion of 3Q coherence are performed by square RIACT elements. Fig. 1c and d implement shaped RIACT pulses for the first or both RIACT steps, respectively. We are concerned with spin dynamics of coherence transfer and focus on isotropic 1D MQMAS spectra. Versions of the above sequences are in routine use to provide pure phase 2D-MQMAS spectra [3,25], but the sequences in Fig. 1 are best suited for studying fundamental mechanisms of coherence transfer.

All numerical simulations were carried out using the GAMMA simulation platform [26]. Although the experiments reported here were performed at 14.1 T, all numerical simulations were based on a ^{23}Na Larmor frequency of 105 MHz (9.4 T, 400 MHz for ^{1}H) which was chosen to reflect the most general and common conditions possible, as well as to be a more challenging test of the proposed methodology.

4. Results and discussion

The initial benefit of the RIACT method was to enhance the sensitivity and quantitative accuracy of MQMAS spectra when measuring sites possessing large quadrupole couplings [14]. Performance characteristics of RIACT for small or very small quadrupole couplings were not explored in detail, and this study focuses specifically on this case.

We first explore simulations of the excitation of triple quantum coherence for spin 3/2 nuclei during magic-angle spinning, given an initial condition of central transition coherence. In Fig. 2, we show the appearance of triple quantum coherence over the course of one rotor period for a spin 3/2 nucleus as a function of several r.f. powers and assuming e^2qQ/h =1.0 MHz. High frequency oscillations occur early in the pulse evolution that are consistent with r.f. driven nutation since the period of oscillation decreases as the r.f. power increases. These oscillations are superimposed on the adiabatic transfer. For $\omega_1/2\pi$ = 50 kHz, the appearance of triple quantum coherence is principally determined by the adiabatic process, while for $\omega_1/2\pi$ = 150 kHz the nutation process dominates; these observations qualitatively support our interpretation of Eq. (6) that nutation will only play a minor role in stimulating 3Q coherence when r.f. powers are low but can become significant as ω_1 increases. It is possible to estimate the initial nutation frequency from the first complete period of oscillation in the simulations. By this simple approach which focuses on very short times we find for example: $\nu_{nut,100}/\sqrt{3} \cong 111$kHz, $\nu_{nut,150}/\sqrt{3} \cong 147$kHz,, $\nu_{nut,200}/\sqrt{3} \cong 193$kHz, $\nu_{nut,300}/\sqrt{3} \cong 311$kHz (data not shown for last two cases) which supports the interpretation of Eq. (10) that the initial 3Q nutation rate be on the order of $\sqrt{3}\omega_1$. We note again that Eq. (10) is not intended to be a realistic presentation of 3Q nutation of central transition coherence over any meaningful time period. A closely related test is shown in Fig. 3, in which the triple quantum excitation is simulated for a fixed r.f. power of $\omega_1/2\pi$ = 150 kHz for several quadrupole couplings. All other conditions for Fig. 3 are the same as in Fig. 2. As the quadrupole coupling decreases, oscillations from nutation increase significantly in intensity, but the initial period of oscillation is the same in every case, again showing that these oscillations arise from r.f. driven 3Q excitation.

Figs. 2 and 3 confirm the superposition of nutation and adiabatic 3Q excitation processes predicted from the prior analysis of the r.f. Hamiltonian, and show that high r.f. powers promote the nutation mechanism. However high r.f. powers are strictly needed to obtain good performance of adiabatic pulses for the broadest possible range of quadrupole couplings [14]. Sculpting the r.f. amplitude may allow for simultaneously suppressing 3Q nutation processes while maintaining the overall performance of the adiabatic transfer. A basic proof of principle test is a linearly ramped pulse amplitude which should inhibit nutation efficiency early in the pulse and allow adiabatic transfer as the pulse amplitude increases. The simulations of Fig. 2 are repeated in Fig. 4 using a lin-

ear ramp pulse amplitude profile for the duration of one rotor period. Importantly, nutation at the beginning of the pulse is essentially abolished, and nutation oscillations throughout the rotor period are significantly attenuated as well in comparison to Fig. 2.

Assuming a perfectly selective pulse on the central transition, the initial condition we must consider is $\rho(0) = \mathbf{I}_X^{23} + 3\mathbf{I}_Z^{14}$. Figs. 2 and 3 explore 3Q nutation of $\rho(0) = \mathbf{I}_X^{23}$, and we repeat this analysis for an initial condition of $\rho(0) = 3\mathbf{I}_Z^{14}$. We have noted earlier that high r.f. powers will also favor nutation in the triple quantum subspace (i.e. $\rho(0) = \mathbf{I}_Z^{14} \rightarrow \rho(t) = \mathbf{I}_X^{14}$); simulations showing typical behavior of this nutation mechanism are given in Fig. 5a, where the initial condition is only triple quantum polarization. Simulations in Fig. 5b show that the nutation in the triple quantum subspace is significantly attenuated (ca. 25%) for the same linearly ramped pulse amplitude used in Fig. 3.

Taking the results of Figs. 4 and 5 together, pulse amplitude sculpting can selectively favor adiabatic transfer while inhibiting nutation in both the central transition and triple quantum subspaces. The linear ramp is only a naiive proof of principle and has undesirable performance characteristics. Note in Fig. 4, for example, that the position of maximum 3Q coherence excitation is a sensitive function of the r.f. power. We next undertook numerical simulations to search simple functional spaces that featured monotonically increasing r.f. power; the performance of shaped pulses was evaluated empirically, with emphasis on maximizing 3Q coherence excitation while suppressing nutation oscillations. Additional criteria in screening pulse shapes included inspecting the offset dependence and quadrupole coupling dependence of the coherence transfer. In the course of these optimizations, an additional criterion emerged that the amplitude should decrease near the end of the pulse duration since nutation processes were often observed arising near the end of pulses (which is evident also in Figs. 4 and 5). The result of this empirical search was to identify a pulse amplitude defined by a truncated sine wave (spanning 0–0.8π over one third of the rotor period) that exhibits good adiabatic coherence transfer and significant attenuation of nutation mechanisms (see Fig. 2c–d for a depiction of the adiabatic pulse shape). An objective numerical optimization of the pulse shape is a nontrivial task and was outside the scope of this study, and further optimizations of the pulse shape are likely still possible.

The truncated sine amplitude profile was determined for adiabatic triple quantum coherence excitation; the pulse shape need only be reversed (see Fig. 2d) to apply to the reconversion of 3Q- to central transition coherence since adiabatic transfer is a symmetric process. Alternately, we can rationalize that for multi-quantum reconversion we must have a low r.f. power at the end of the pulse to inhibit nutation processes.

The performance of the shaped pulse obtained here is well illustrated by examining the appearance of triple quantum coherence as a function of quadrupole coupling in Fig. 6. First, in comparing the performance of square pulses of duration $\tau_R/4$ in Fig. 6a–c (dashed lines), increasing the r.f. power decreases the excitation of triple quantum coherence for quadrupole couplings e^2qQ/h < 2.0 MHz. This does not represent a contradiction of the adiabaticity parameter, but rather is a consequence of more favorable competing nutation processes for small quadrupole couplings at higher r.f. powers. The simulations for increasing r.f. powers in Fig. 6a–c indicate that the quantitative accuracy of the adiabatic transfer will be adversely affected by competing nutation processes for square adiabatic pulses, and further that overall sensitivity will be reduced for nuclei with small quadrupole couplings. As r.f. power increases in Fig. 6a–c, the shaped pulse of duration $\tau_R/3$ is seen to improve the triple quantum excitation for e^2qQ/h < 2.0 MHz compared to the square pulse, and to yield a more uniform excitation over a broader range of quadrupole couplings. A simple calculation shows that the shaped pulse, although of longer duration, applies about 5% less net power than the shorter square pulse, supporting that the improvement in the coherence transfer with less net power must result from manipulation of coherence transfer pathways. In contrast, when the r.f. power is so low that nutation effects are of no concern, i.e. $\omega_1/2\pi$ = 50 kHz in Fig. 6a, the shaped pulse offers no advantage and the lower net power

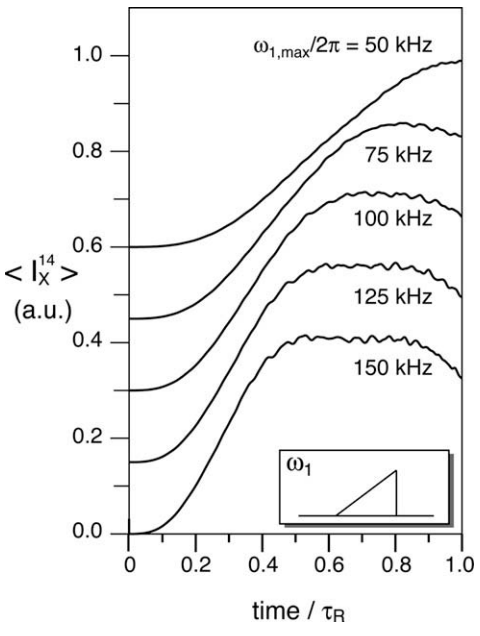

Fig. 4. Numerical simulations of triple quantum coherence excitation using the identical conditions as in Fig. 2, except for linearly increasing the r.f. power over the course of a rotor period to the maximum values indicated of 50, 75, 100, 125, and 150 kHz. Nutation oscillations observed in Fig. 2 are nearly eliminated in these simulations.

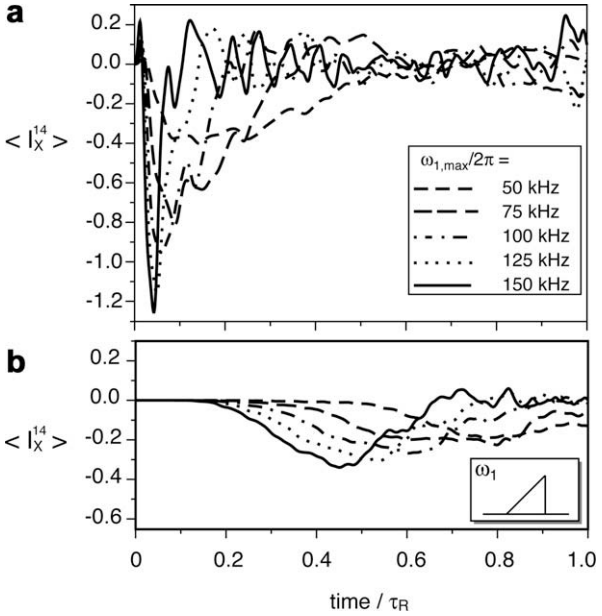

Fig. 5. Numerical simulations of triple quantum coherence excitation using an initial condition of only triple quantum polarization (i.e. $\rho(0) = \mathbf{I}_Z^{14}$) and using only the low order quadrupole coupling in the Hamiltonian. Panel (a) shows the creation of triple quantum coherence using a square pulse for the duration of a rotor period, and shows that coherence transfer by nutation increases significantly with r.f. power. Panel (b) shows significant attenuation of triple quantum excitation by the use of a linearly ramped pulse amplitude. The simulations also assumed 10 kHz MAS, e^2qQ/h = 1.0 MHz, η = 0.0, and 2000 crystal orientations.

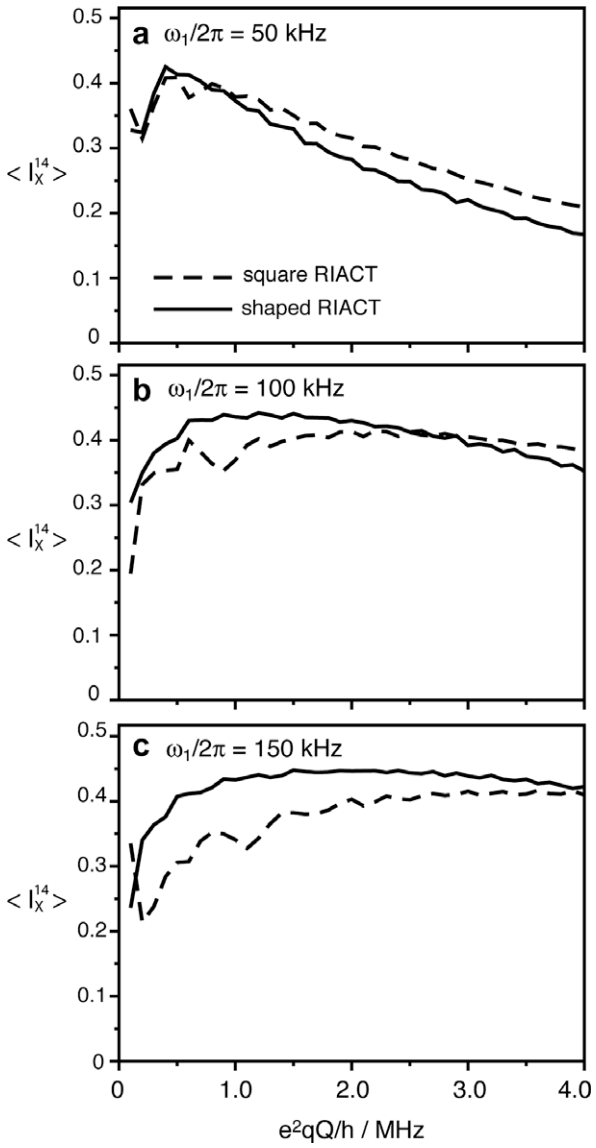

Fig. 6. Numerical simulations of the dependence of triple quantum excitation by RIACT on the quadrupole coupling for square and shaped RIACT, where the shaped pulse is the empirically optimized truncated sine wave described in the text. The first and second order corrections to the quadrupolar Hamiltonian were used since the simulation treats cases up to e^2qQ/h = 4.0 MHz. For each value of e^2qQ/h, the isotropic shift was computed and the r.f. pulse was applied on resonance with the isotropic shift (sum of Zeeman and second order quadrupolar isotropic shifts). The simulations also assumed 10 kHz MAS, η = 0.0, and 1000 crystal orientations (separate tests showed no difference with 2000 orientations).

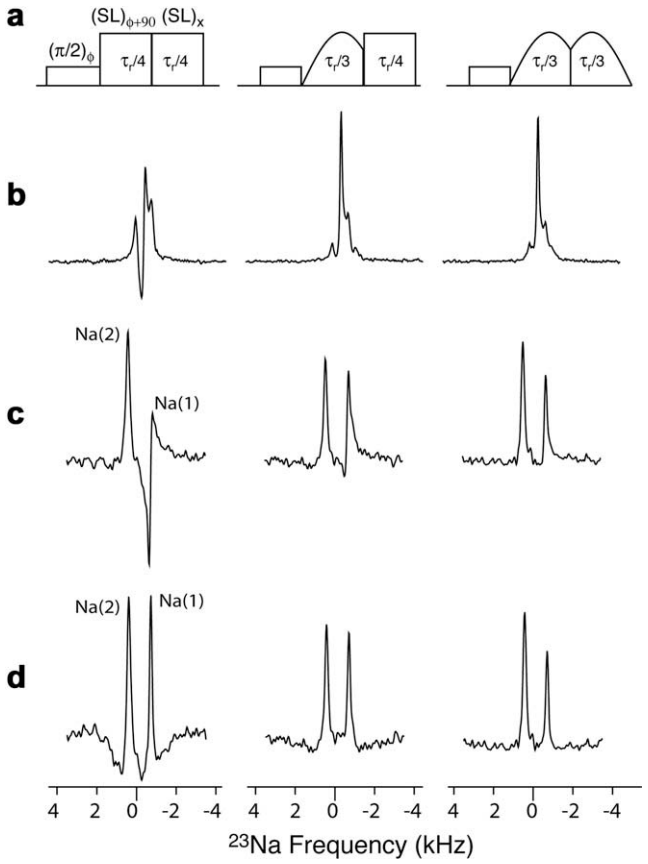

Fig. 7. In row (a) pulse sequences are given for (b) triple quantum filtered and (c–d) MQMAS spectra of sodium pyrophosphate ($Na_4P_2O_7$–$10H_2O$). The MAS rate was 13 kHz and the indirect evolution period was rotor synchronized (Δt_1 = 1/13000). Non phase-corrected spectra are shown in row (c) to illustrate the phase twist for Na(1), which experiences significant nutation interference during the RIACT pulses. The isotropic spectra in row (d) were obtained just by applying a phase correction to the corresponding spectra (c). The r.f. power levels were $\omega_1/2\pi$ = 125 kHz, except for the soft $\pi/2$ pulse, which had a power of $\omega_1/2\pi$ = 30 kHz.

likely contributes to the slightly poorer performance of the shaped RIACT pulse in Fig. 6a.

The deficiencies of square RIACT pulses applied to sites with e^2qQ/h < 2.0 MHz are experimentally illustrated in a number of ^{23}Na spectra of sodium pyrophosphate in Fig. 7. Sodium pyrophosphate consists of two inequivalent sodium sites in a 1:1 ratio, and possessing significantly different quadrupole coupling magnitudes. Specifically, Na(1) has an extremely small e^2qQ/h with an upper limit of 0.2 MHz, while Na(2) has a moderate coupling of e^2qQ/h = 2.0 MHz [14]. The left column of Fig. 7 gives results using square RIACT pulses of duration $\tau_r/4$: the first 1D slice of the MQMAS data (Fig. 7b: no evolution of 3Q coherence between the two spin-locking pulses, a triple quantum filter) exhibits significant negative intensity over part of the line shape. The isotropic MQMAS spectrum without phase correction is given for all cases in the third row (Fig. 7c), and shows an approximate 90° phase shift for Na(1) compared to Na(2) when square RIACT pulses are employed for 3Q excitation and reconversion; phasing of this spectrum (Fig. 7d) results in severe baseline roll. The 90° phase shift of Na(1) in the unphased square pulse RIACT MQMAS spectrum is significant since it demonstrates that 3Q coherence for Na(1) was largely generated by a nutation mechanism in the first RIACT pulse since it is phase encoded by ϕ+90, whereas Na(2) results primarily from the adiabatic mechanism and is phase encoded by the ϕ phase of the initial selective $\pi/2$ pulse. In other words, the triple quantum excitation of Na(1) is governed primarily by a nutation mechanism in the triple quantum subspace according to Eq. (6).

The reconversion efficiency of 3Q to central transition coherence by nutation is poor, [1,18,19] especially for long pulse durations (e.g $\tau_r/4$) so that the multi-quantum reconversion for both Na(1) and Na(2) is likely to proceed mainly by an adiabatic path, even with the use of square pulses. The middle column of Fig. 7 tests this prediction by substituting the shaped pulse for the initial excitation step only. Indeed the triple quantum filtered spectrum no longer shows the large negative component, and the phase twist in the 1D isotropic MQMAS spectrum has been significantly attenuated. Nevertheless, undesirable baseline roll results in the properly phased 1D MQMAS spectrum when only the first RIACT pulse employs the shape. When both adiabatic pulses use the shaped amplitude profile, the phase twist is nearly abolished in the unphased spectrum (Fig. 7c) and can be corrected easily with

little or no baseline distortion (Fig. 7d). In comparing Fig. 7d to the quadrupole dependence of the shaped pulses in Fig. 6, we see that Na(1) possesses such a small quadrupole coupling that it lies outside the region of uniform triple quantum excitation. In other words, despite the improvements obtained with the shaped pulse, Fig. 7d confirms the simulations of Fig. 6, that Na(1) will have a lower net amplitude than Na(2).

The simulations in Fig. 6 indicate that the shaped adiabatic pulses should lead to significantly better quantitative accuracy in MQMAS experiments in comparison to square adiabatic pulses in the regime of e^2qQ/h = [0.5–4 MHz], but particularly when samples include sites with small quadrupole couplings. We prepared 50:50% mixtures of Na_2SO_4:$NaNO_2$ and Na_2SO_4:$NaNO_3$ where Na_2SO_4 exhibits a mid-range coupling (e^2qQ/h = 2.6 MHz, η = 0.6) [27] and smaller couplings are exhibited by $NaNO_2$ (e^2qQ/η = 1.10 MHz, η = 0.11) [28] and $NaNO_3$ (e^2qQ/h = 0.334 MHz, η = 0) [29]. Isotropic ^{23}Na MQMAS spectra for these mixtures are shown in Fig. 8. For the mixture of sodium sulfate and sodium nitrite in Fig. 8a, the MQMAS spectrum using square RIACT pulses (Fig. 1b) exhibits a ratio of signal integrals of 1.0:0.65 for Na_2SO_4:$NaNO_2$ and using an r.f. power of about $\omega_1/2\pi$ = 125 kHz. The use of the shaped pulses (Fig. 1d) leaves the intensity of the sodium sulfate isotropic line essentially unchanged in Fig. 8a, but leads to a significant increase in the sodium nitrite signal. Noticing that the sodium nitrite isotropic line is somewhat broader, the integrals of the isotropic lines obtained from using shaped RIACT pulses are 0.98:1.0 for Na_2SO_4:$NaNO_2$. In the mixture of Na_2SO_4:$NaNO_3$, the MQMAS spectrum using square RIACT pulses exhibited a substantial phase twist due to the sodium nitrate line. Phasing and spline fitting to correct the baseline were performed prior to obtaining integrals of 1.0:0.41 for Na_2SO_4:$NaNO_3$ (Fig. 8b, dashed line). The use of shaped pulses restores a significant amount of intensity to the isotropic $NaNO_3$ line without perturbing the intensity of the Na_2SO_4 line, yielding a ratio of integrals of 1.0:0.81 for Na_2SO_4:$NaNO_3$. Some residual phase twist remained in analogy to the case with pyrosphosphate. Although the quadrupole coupling of $NaNO_3$ is so small that it falls outside of the region of uniform excitation of the shaped pulse (Fig. 6), an additional factor is that we noted an extremely long T_1 for ^{23}Na in $NaNO_3$; despite the use of a 20 s recycle time, minor T_1 losses for the $NaNO_3$ signal likely occurred. Fig. 8b shows that the use of the shaped pulses achieves near quantitative accuracy for two sites that differ in the quadrupole coupling by almost an order of magnitude.

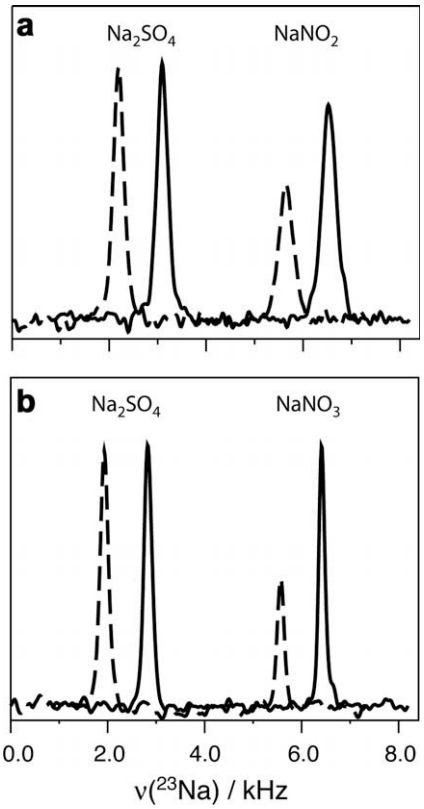

Fig. 8. Isotropic ^{23}Na MQMAS spectra for 50%:50% mixtures of (a) sodium sulfate and sodium nitrite and (b) sodium sulfate and sodium nitrate. Quadrupole parameters for these samples are given in the text. The RIACT MQMAS spectra using two square RIACT pulses of duration $\tau_R/4$ are represented with dashed lines, while solid lines correspond to MQMAS spectra acquired with two shaped RIACT pulses of duration $\tau_R/3$ each. In (a) and (b), using square RIACT pulses falsely suggests about 2:1 ratios among the components. Using shaped RIACT pulses significantly corrects the intensities of the $NaNO_2$ and $NaNO_3$ lines, while leaving the Na_2SO_4 lines unperturbed. All high power pulses were $\omega_1/2\pi$ = 125 kHz. As in Fig. 7, the MAS rate and indirect spectral width were both 13 kHz, and 72 t_1 increments were obtained.

Additional experiments were performed on $NaNO_2$ as shown in Fig. 9. In Fig. 9a, the isotropic MQMAS line from the use of $\tau_R/4$ square RIACT pulses is displayed, while Fig. 9b gives the isotropic line when a $\tau_R/3$ shaped pulse is used in just the excitation step. As we found also with the pyrophosphate experiments, a substantial improvement is seen with just the first substitution, while a more modest increase in the sensitivity is obtained upon using the shaped pulse for the second step as well (Fig. 9c).

MQMAS spectra that incorporate a RIACT element for triple quantum excitation can be improved by preparing a state of enhanced central transition polarization prior to the application of the selective $\pi/2$ pulse. These methods may be based on employing a pulse train such as $(P(x) -\tau - P(\bar{x}))_n$ where the interval τ, number of iterations n, and pulse duration P() can all be fine tuned; this approach is frequently termed fast amplitude modulation (FAM) [30–32]. More recently the use of hyperbolic secant pulses has been shown to provide enhancements of central transition polarization near the theoretical limit of a factor of 3 for S = 3/2 nuclei [33,34]. We show the former approach of phase-alternated pulses to enhance the isotropic MQMAS spectra of $NaNO_2$ in Fig. 9d and e, where Fig. 9d employs square adiabatic pulses and Fig. 9e employs shaped adiabatic pulses. Significant enhancements are observed when comparing Fig. 9d and e, showing that the shaped pulse method is complementary with methods for enhancing the central transition coherence. Although

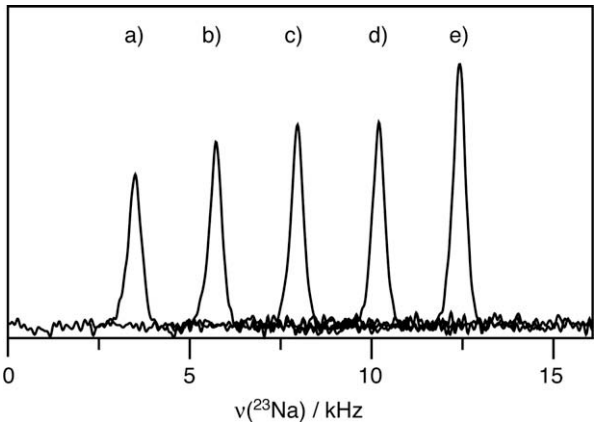

Fig. 9. Series of isotropic ^{23}Na MQMAS spectra acquired for $NaNO_2$. The MAS rate was 18 kHz and the indirect evolution increments were matched to the rotor cycle. Parts (a–c) were obtained with the sequences of Fig. 1b–d, respectively. The use of phase alternating pulse trains (a.k.a. fast amplitude modulation, FAM) to enhance the central transition polarization prior the application of the selective $\pi/2$ pulse is shown in (d) and (e) for square and shaped pulses respectively. All high power pulses were $\omega_1/2\pi$ = 125 kHz.

the principal enhancement in this case results from the increased central transition polarization, it may be suggested that reducing the triple quantum polarization will reduce the subsequent competing nutation process in the triple quantum subspace during the adiabatic pulse and thereby improve the performance of the adiabatic pulse. The highest sensitivity available for MQMAS spectra is obtained by hybrid pulse sequences that incorporate RIACT in the 3Q excitation portion (e.g. FAM-RIACT-FAM sequence [32]), with the HS-RIACT-HS hybrid sequence yielding the highest sensitivity at this time [35]. The shaped RIACT methodology here can be seen from Fig. 9 to extend (albeit modestly) the sensitivity of MQMAS spectroscopy of spin 3/2 nuclei.

Finally, we investigate the dependence of MQMAS spectroscopy on MAS rate for nutation, square RIACT and shaped RIACT methods. The square and shaped RIACT methods are given in Fig. 1b and Fig. 1d, respectively, while the nutation sequence consists of two hard pulses with appropriate phase cycling to select for the excitation and reconversion of triple quantum coherence [1,18,19]. For efficiency, we recorded in each case only a 1D spectrum with no evolution time between the triple quantum excitation and reconversion steps, and measured the integrated intensities of these triple quantum filtered spectra. Since total signal intensity is always directly proportional to the value of the first point, the spectrum with no evolution is an accurate representation of the intensity of the isotropic MQMAS signal since it represents the first "point" of the isotropic FID. Integrations of signal intensity are shown for Na_2SO_4 and $NaNO_2$ over the range of 9–25 kHz MAS rates in Fig. 10. These data confirm that both square and shaped adiabatic transfers are insensitive to the MAS rate since it is relatively straightforward to achieve high r.f. power levels on modern commercial probe-heads in order to satisfy the adiabaticy parameter a. Fig. 10a–b also show the expected decrease in nutation sensitivity as a function of increasing MAS rate, which is attributable to improved averaging of the low order quadrupole coupling which transforms as a second rank tensor under magic-angle spinning.

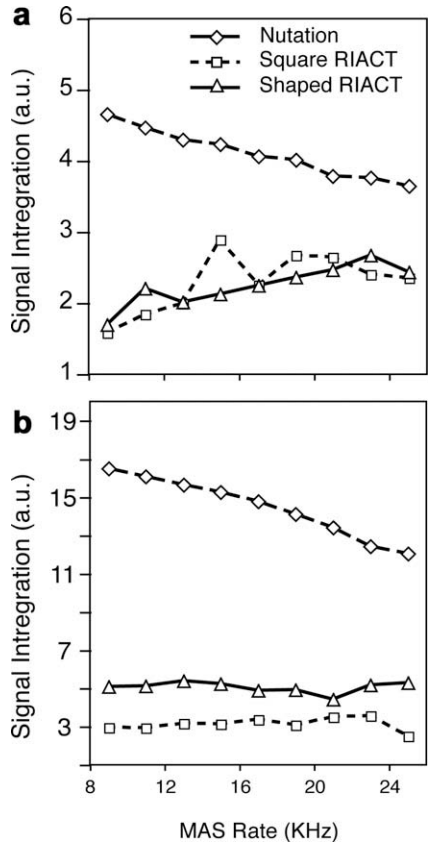

Fig. 10. Experimental analysis of the MAS dependence of the first 1D spectrum (a.k.a. slice) of an MQMAS experiment by nutation (diamonds), square RIACT (triangles) and shaped RIACT (squares). The integral of the first slice of an MQMAS experiment is directly proportional to the intensity of the isotropic line. Part (a) used Na_2SO_4 and (b) used $NaNO_2$. Both square and shaped RIACT schemes are insensitive to the MAS rate, while nutation is attenuated with increase MAS rate. All high power pulses were $\omega_1/2\pi$ = 125 kHz.

5. Conclusion

Nutation mechanisms operating on the triple quantum subspace and on central transition coherence are both shown to interfere with rotation induced adiabatic coherence transfers in spin 3/2 nuclei. Isotropic MQMAS spectra obtained with square RIACT pulses will exhibit phase twist, loss of sensitivity and loss of quantitative accuracy when applied to sites with small quadrupole couplings. A shaped amplitude pulse is presented which nearly abolishes nutation of the central transition coherence, while significantly reducing nutation of triple quantum polarization. Using the shaped pulse in both steps of the MQMAS experiment provides quantitative accuracy over a broad range of quadrupole couplings, reduces or eliminates phase twist, and provides overall signal enhancements. The shaped adiabatic pulse is shown to be insensitive to MAS rate, but requires high r.f. powers for optimal use.

The use of shaped pulses in RIACT MQMAS can extend the sensitivity limit of isotropic MQMAS spectra and should be useful in the study of metal ions bound to biomacromolecules. The more efficient coherence transfer of the shaped pulse may also enhance distance measurement techniques which depend on adiabatic processes [36,37]. Further optimization of RIACT processes should be feasible by extended numerical searches for improved pulse shapes, or also by preparing tailored spin states prior to RIACT modules.

Acknowledgments

We thank Matthias Ernst for valuable assistance with the implementation of gamma. The 14.1 T Varian spectrometer was acquired with the support of the NSF (MRI-0521108) and Bucknell University.

Appendix A

A.1. 3Q nutation for $\omega_1 > \omega_Q$

As noted in the theory section, for the case $\omega_Q > \omega_1$, the 3Q nutation was derived by Vega [15] by tilting the 1–2 and 3–4 terms in Eq. (1) by:

$$H_T^Q = e^{-i\theta_{12}\mathbf{I}_Y^{12}} e^{-i\theta_{34}\mathbf{I}_Y^{34}} H e^{i\theta_{34}\mathbf{I}_Y^{34}} e^{i\theta_{12}\mathbf{I}_Y^{12}}, \theta_{12} = -\theta_{34} = \tan^{-1}(\sqrt{3}\omega_1/\omega_Q). \tag{A1}$$

In the limit $\omega_Q > \omega_1$, the inverse tangent approaches 0 and allows for many approximations to simplify H_T^Q and the tilted density operator. Similarly, we may tilt Eq. (1) such that the 1-2 and 3-4 subspaces lie on their respective *x*-axes:

$$H_T^Q = e^{-i\theta_{12}\mathbf{I}_Y^{12}} e^{-i\theta_{34}\mathbf{I}_Y^{34}} H_{LAB}^Q e^{i\theta_{34}\mathbf{I}_Y^{34}} e^{i\theta_{12}\mathbf{I}_Y^{12}}, \theta_{12} = -\theta_{34} = \tan^{-1}\left(\omega_Q/\sqrt{3}\omega_1\right). \tag{A2}$$

The resulting tilted Hamiltonian (with $\theta = \theta_{12} = -\theta_{34}$) is

$$H_T^Q = \omega_{eff}(\mathbf{I}_X^{12} + \mathbf{I}_X^{34}) - 2\omega_1((\cos^2\frac{\theta}{2}\mathbf{I}_X^{23} - \cos\frac{\theta}{2}\sin\frac{\theta}{2}\mathbf{I}_X^{13}) + (-\sin\frac{\theta}{2}\cos\frac{\theta}{2}\mathbf{I}_X^{24} + \sin^2\frac{\theta}{2}\mathbf{I}_X^{14})). \tag{A3}$$

Turning to the initial density operator, the equilibrium polarization is invariant to the rotating frame transformation, and the tilted density operator becomes

$$\rho_T(0) = e^{-i\theta_{12}\mathbf{I}_Y^{12}} e^{-i\theta_{34}\mathbf{I}_Y^{34}} (\mathbf{I}_Z^{23} + 3\mathbf{I}_Z^{14}) e^{i\theta_{34}\mathbf{I}_Y^{34}} e^{i\theta_{12}\mathbf{I}_Y^{12}}$$
$$= \cos^2\frac{\theta}{2}\mathbf{I}_Z^{23} + 2\cos\frac{\theta}{2}\sin\frac{\theta}{2}\mathbf{I}_X^{12} + 2\sin\frac{\theta}{2}\mathbf{I}_X^{34} + 3\cos^2\frac{\theta}{2}\mathbf{I}_Z^{14}. \quad \text{(A4)}$$

The limiting constraint, $\omega_1 > \omega_Q$, is now applied:

$$\lim_{(\omega_1/\omega_Q)\to 0}(\theta = \tan^{-1}(\sqrt{3}\omega_1)) = 0. \quad \text{(A5)}$$

Eq. (A4) then acquires the expected form:

$$\rho_T(0) \approx \mathbf{I}_Z^{23} + 3\mathbf{I}_Z^{14}. \quad \text{(A6)}$$

Approximating $\sin\frac{\theta}{2} \approx \frac{\theta}{2}$ in Eq. (A3) yields

$$H_T^Q = -2\omega_1\mathbf{I}_X^{23} - \frac{\omega_Q^2}{6\omega_1}\mathbf{I}_X^{14} + \omega_{eff}(\mathbf{I}_X^{12} + \mathbf{I}_X^{34}) - \frac{\omega_Q}{\sqrt{3}}(\mathbf{I}_X^{13} + \mathbf{I}_X^{24}). \quad \text{(A7)}$$

If the initial condition is equilibrium polarization (i.e. Eq. (A6)) then 3Q coherence will be obtained by nutation in the triple quantum subspace ($-\frac{\omega_Q^2}{6\omega_1}\mathbf{I}_X^{14}$), a regime which was empirically explored elsewhere [7]. The terms $(\mathbf{I}_X^{12} + \mathbf{I}_X^{34})$ and $(\mathbf{I}_X^{13} + \mathbf{I}_X^{24})$ will not create 3Q coherence. If we apply Eq. (A7) to an initial condition of $\mathbf{I}_X^{23}$ then the terms $\omega_{eff}(\mathbf{I}_X^{12} + \mathbf{I}_X^{34})$ and $(\mathbf{I}_X^{13} + \mathbf{I}_X^{24})$ are both capable of yielding 3Q coherence. Further discussion of Eq. (A7) is given in the text.

References

[1] A. Medek, J.S. Harwood, L. Frydman, Multiple-quantum magic-angle spinning NMR: a new method for the study of quadrupolar nuclei in solids, J. Am. Chem. Soc. 117 (51) (1995) 12779–12787.
[2] L. Frydman, J.S. Harwood, Isotropic spectra of half-integer quadrupolar spins from bidimensional magic-angle spinning NMR, J. Am. Chem. Soc. 117 (1995) 5367–5368.
[3] A. Goldbourt, P.K. Madhu, Multiple-Quantum Magic-Angle Spinning: high-resolution solid-state NMR of half-integer spin quadrupolar nuclei, Ann. Rep. NMR Spec. 54 (2005) 810153.
[4] J. Kanellopoulos, D. Freude, A. Kentgens, A practical comparison of MQMAS techniques, Solid State Nucl. Magn. Reson. 32 (2007) 99–108.
[5] Z. Gan, Satellite transition magic-angle spinning nuclear magnetic resonance spectroscopy of half-integer quadrupolar nuclei, J. Chem. Phys. 114 (2001) 10845–10853.
[6] Z. Gan, Isotropic NMR spectra half-integer quadrupolar nuclei using satellite transitions and magic-angle spinning, J. Am. Chem. Soc. 122 (2000) 3242–3243.
[7] D. Rovnyak, M. Baldus, G. Wu, N. Hud, J. Feigon, R.G. Griffin, Localization of 23Na+ in a DNA quadruplex by high-field solid state NMR, J. Am. Chem. Soc. 122 (2000) 11423–11429.
[8] A. Wong, J.C. Fettinger, S.L. Forman, J.T. Davis, G. Wu, The sodium ions inside a lipophilic G-quadruplex channel as probed by solid-state 23Na NMR, J. Am. Chem. Soc. 124 (5) (2002) 742–743.
[9] G. Wu, A. Wong, Direct detection of the bound sodium ions in self-assembled 5'-GMP gels: a solid-state 23Na NMR approach, Chem. Commun. (2001) 2658–2659.
[10] G. Wu, A. Wong, Solid-state 23Na NMR determination of the number and coordination of sodium cations bound to Oxytricha nova telomere repeat d(G4T4G4), Biochem. Biophys. Res. Commun. 323 (2004) 1139–1144.
[11] S. Ashbrook, S. Wimperis, Satellite-transition MAS NMR of spin *I*=3/2, 5/2, 7/2 and 9/2 nuclei: sensitivity, resolution, and practical implementation, J. Magn. Reson. 156 (2002) 269–281.
[12] N.G. Dowell, S. Ashbrook, S. Wimperis, Satellite transition MAS NMR of low-gamma nuclei at natural abundance. sensitivity, practical implementation, and application to 39-K (I=3/2) and 25-Mg (I=5/2), J. Phys. Chem. B 108 (2004) 13292–13299.
[13] A.J. Vega, MAS NMR spin locking of half-integer quadrupolar nuclei, Magn. Reson. 96 (1992) 50–68.
[14] G. Wu, D. Rovnyak, R.G. Griffin, Quantitative multiple-quantum magic-angle-spinning NMR spectroscopy of quadrupolar nuclei in solids, J. Am. Chem. Soc. 118 (39) (1996) 9326–9332.
[15] S. Vega, Fictitious spin 1/2 operator formalism for multiple quantum NMR, J. Chem. Phys. 68 (12) (1978) 5518–5527.
[16] A. Wokaun, R.R. Ernst, Selective excitation and detection in multilevel spin systems: application of single transition operators, J. Chem. Phys. 67 (4) (1977) 1752–1758.
[17] S. Vega, Y. Naor, Triple quantum NMR on spin systems with *I*=3/2 in solids, J. Chem. Phys. 75 (1) (1981) 75–86.
[18] J.P. Amoureux, C. Fernandez, L. Frydman, Optimized multiple-quantum magic-angle spinning NMR experiments on half-integer quadrupoles, Chem. Phys. Lett. 259 (1996) 347–355.
[19] G. Wu, D. Rovnyak, B. Sun, R.G. Griffin, High-resolution multiple quantum MAS NMR spectroscopy of half-integer quadrupolar nuclei, Chem. Phys. Lett. 249 (1995) 210–217.
[20] A.J. Vega, CP/MAS of quadrupolar *S*=3/2 nuclei, Solid State Nucl. Magn. Reson. 1 (1992) 17–32.
[21] M. Baldus, D. Rovnyak, R.G. Griffin, Radio-frequency-mediated dipolar recoupling among half-integer quadrupolar spins, J. Chem. Phys. 112 (13) (2000) 5902–5909.
[22] D. Rovnyak, M. Baldus, R.G. Griffin, Multiple-quantum cross polarization in quadrupolar spin systems during magic-angle spinning, J. Magn. Reson. 142 (2000) 145–152.
[23] J.C. Hoch, A.S. Stern, NMR Data Processing, Wiley Liss, New York, 1996.
[24] K.H. Lim, C.P. Grey, Analysis of the anisotropic dimension in the RIACT(II) multiple quantum MAS NMR experiment for *I*=3/2 nuclei, Solid State Nucl. Magn. Reson. 13 (1998) 101–112.
[25] S.P. Brown, S. Wimperis, Two-dimensional multiple-quantum MAS NMR of quadrupolar nuclei: a comparison of methods, J. Magn. Reson. 128 (1997) 42–62.
[26] S.A. Smith, T.O. Levante, B.H. Meier, R.R. Ernst, Computer simulations in magnetic resonance. An object oriented programming approach, J. Magn. Reson. A 106 (1994) 75–105.
[27] E. Oldfield, S. Schramm, M.D. Meadows, K.A. Smith, R.A. Kinsey, J. Ackerman, High-resolution NMR spectroscopy of quadrupolar nuclei in solids: sodium salts, J. Am. Chem. Soc. 104 (1982) 919–920.
[28] A. Weiss, The resonance spectrum of the nuclear spin of Na-23 in single crystals of sodium nitrite, $NaNO_2$, Z. Naturforsch. 15A (1960) 536–542.
[29] R. Pound, Nuclear electric quadrupole interactions in crystals, Phys. Rev. 79 (4) (1950) 685–702.
[30] H.-T. Kwak, S. Prasad, Z. Yao, P.J. Grandinetti, J.R. Sachleben, L. Emsley, Enhanced sensitivity in RIACT/MQ-MAS NMR experiments using rotor assisted population transfer, J. Magn. Reson. 150 (2001) 71–80.
[31] K.H. Lim, T. Charpentier, A. Pines, Efficient triple-quantum excitation in modified RIACT MQMAS NMR for *I*=3/2 nuclei, J. Magn. Reson. 154 (2002) 196–204.
[32] P.K. Madhu, M.H. Levitt, Signal enhancement in the triple-quantum magic-angle spinning NMR of spins=3/2 in solids: the FAM-RIACT-FAM sequences, J. Magn. Reson. 155 (2002) 150–155.
[33] T.T. Nakashima, R. Wasylishen, R. Siegel, K.J. Ooms, Sensitivity enhancement of solid-state NMR spectra of half-integer spin quadrupolar nuclei: double- or single- frequency sweeps? Insights from the hyperbolic secant experiment, Chem. Phys. Lett. 450 (2008) 417–421.
[34] R. Siegel, T.T. Nakashima, R. Wasylishen, Signal enhancement of NMR spectra of half-integer quadrupolar nuclei in solids using hyperbolic secant pulses, Chem. Phys. Lett. 388 (2004) 441–445.
[35] R. Siegel, T.T. Nakashima, R. Wasylishen, Sensitivity enhancement of MQMAS NMR spectra of spin 3/2 nuclei using hyperbolic secant pulses, Chem. Phys. Lett. 403 (2005) 353–358.
[36] T. Gullion, Measurement of dipolar interactions between spin-1/2 and quadrupolar nuclei by rotational-echo, adiabatic-passage, double-resonance NMR, Chem. Phys. Lett. 246 (1995) 325–330.
[37] T. Gullion, Detecting 13C–17O dipolar interactions by rotational-echo, adiabatic-passage, double-resonance NMR, J. Magn. Reson. A 117 (1995) 326–329.